1 **Integration and conversion of supercritical carbon dioxide coal-fired power cycle**

2 **and high efficiency energy storage cycle: feasibility analysis based on a three-step**

3 **strategy**

4 D L Yang [a], G H Tang [a, **], K H Luo [b, *,**], Y H Fan [a], X L Li [a], Q Sheng [c]

5 [a] MOE Key Laboratory of Thermo-Fluid Science and Engineering, School of Energy and Power

6 Engineering, Xi'an Jiaotong University, Xi'an 710049, China

7 [b] Dept of Mechanical Engineering, University College London, London WC1E 7JE, United Kingdom

8 [c] School of Mathematics, Computer Science and Engineering, City University of London,

9 London EC1V 0HB, United Kingdom

10 [a, **] Corresponding author. Tel: +86(0)29-82665319 E-mail: ghtang@mail.xjtu.edu.cn

11 [b, *, **] Corresponding author. Tel: +44(0)20-76793916 E-mail: k.luo@ucl.ac.uk

12 * Corresponding author ** The two authors have the same contribution to this study.

13

14 **Abstract**

15 The emission peak/carbon neutrality calls for significantly improved coal-fired power plants.

16 Sustainability of the power plants is critical to meeting the net zero targets in 2050/2060. In this context,

17 it is necessary to investigate the integration and conversion of the supercritical carbon dioxide

18 coal-fired power cycle and the supercritical carbon dioxide energy storage cycle. In this work, the

19 thermodynamic model and performance criteria are firstly presented. After comparison of the two

20 cycles, a three-step strategy for the development of the power cycle is proposed and assessed. First step:

21 when coal still plays an important role as a main energy resource, the integrated tri-compression

22 coal-fired supercritical compressed carbon dioxide energy storage cycle has the highest round-trip

23 efficiency of 56.37%. Second step: with the challenge in utilization of coal energy, a trade-off among

24 the performance criteria must be struck in the integrated cycle with various heat sources. Third step: the

25 adiabatic supercritical compressed carbon dioxide energy storage cycle is proposed, and a high

26 round-trip efficiency of 72.34% is achieved in the split expansion cycle. The present research provides

1   not only a new prospect of the power plants but also design guidance for the supercritical carbon

2   dioxide energy storage cycle.

3

4   **Keywords:** supercritical carbon dioxide; coal-fired power cycle; energy storage cycle; integration and

5   conversion; feasibility analysis; three-step strategy

6

Nomenclature			
e	specific exergy, $kJ \cdot kg^{-1}$	inte	integrated
E	exergy, kW	k	each storage tank
h	specific enthalpy, $kJ \cdot kg^{-1}$	L	exergy loss
$\dot{m}$	S-CO_2 mass flow rate, $kg \cdot s^{-1}$	out	outer
P	pressure, MPa	P	product exergy
Q_h	heat absorption, $kJ \cdot kg^{-1}$	pp	power plant
s	specific entrophy, $kJ \cdot kg^{-1} \cdot K^{-1}$	rt	round-trip
T	temperature, °C	s	isentropic process
V_r	storage volume, m^{-3}	t	turbine
W	shaft work, $kJ \cdot kg^{-1}$	thro	throttle valve
y^{*}	exergy destruction ratio		
		Abbreviations	
Greek letters		C	compressor
ρ	density, $kg \cdot m^{-3}$	G	generator
η	efficiency	HPT	high pressure storage tank
χ	S-CO_2 flow rate extraction ratio	HTR	high temperature recuperator
		LPT	low pressure storage tank
Subscripts		LTR	low temperature recuperator
c	compressor	M	motor
D	exergy destruction	MTR	middle temperature recuperator
E	energy storage	RE	recuperator
F	fuel exergy	T	turbine
i	each component		
in	inner		

7

1. Introduction

Based on the requirements of emission peak and carbon neutrality, the coal-fired power plants will be reduced gradually. However, coal is still one of the main energy resources worldwide [1]. Therefore, the coal-fired power plants should not be abandoned in the near future but improved in a step-by-step approach.

For advanced coal-fired power plants, the supercritical carbon dioxide (S-CO$_2$) Brayton cycle has drawn significant attention as a promising alternative to the traditional steam Rankine cycle, owing to its advantages in efficiency, oxidation rate, compactness and so on [1, 2]. As an emerging technology, the coal-fired S-CO$_2$ power plant is under intensive development while coal still plays an important role as a main energy resource. Therefore, the upgrade of the coal-fired S-CO$_2$ power system still matters. As coal is not an environmentally friendly energy resource, the coal-fired power plants face the prospect of being demolished in the foreseeable future, if without significant improvement, resulting in a waste of all the relevant research investment and upfront costs of the power plants. From a development perspective, the sustainability of the power generation system is critical. This requires examining the potential for the transition of the coal-fired S-CO$_2$ power system into clean energy system rather than being abandoned completely.

Understanding of the coal-fired S-CO$_2$ power system is the foundation for the upgrade of the traditional coal-fired power plants. As a pioneering work, Mecheri and Le Moullec [2, 3] studied the S-CO$_2$ Brayton cycle in a coal-fired power plant and found that reheating and recompression in the Brayton cycle can increase the cycle efficiency up to 47.8%, which is much higher than the steam Rankine cycle. Xu et al. [4] examined the pressure drop of the S-CO$_2$ coal-fired Brayton cycle and found that the large mass flow rate in the power cycle would cause large pressure drop and further reduce the cycle efficiency. Therefore, they proposed the 1/8 principle and partial flow strategy to tackle this problem. Moreover, Sun et al. [5] proposed an overlap energy utilization method to improve S-CO$_2$ Brayton cycle efficiency by using residual heat in the power system. The present authors also have an in-depth understanding of the S-CO$_2$ coal-fired power system. Fan et al. [6, 7] proposed an integration of the S-CO$_2$ Brayton cycle and designed the system based on a multiscale analysis platform. Li et al. [8] proposed an integrated model of the S-CO$_2$ Brayton cycle and PCHE design. Yang et al. [9] established a coupled model of the S-CO$_2$ Brayton cycle and coal-fired furnace. Furthermore, a unified model was

proposed for studying the capacity-dependent configuration of the S-CO$_2$ coal-fired Brayton power cycle [10]. Based on the abovementioned works, the various configurations of the S-CO$_2$ coal-fired Brayton power cycles were found in common with the compressor, turbine, heater, cooler and recuperator. For the sustainability of the power system, the transformation of the system must consider the reusability of the components and the working circuit, in addition to other factors. Therefore, it is crucial to find a clean energy cycle that shares features with the S-CO$_2$ coal-fired cycle.

As is well known, the compressed air energy storage cycle is a typical technology for improving utilization of intermittent renewable energy sources, which is derived from the Brayton cycle [11]. Furthermore, the cycle performance will be improved by using CO$_2$ as the working fluid in the energy storage cycle [12], which suggests that the S-CO$_2$ coal-fired Brayton power cycle may have similarities to the compressed CO$_2$ energy storage cycle. Thus, a review of the energy storage cycle is conducted below.

The development of the CO$_2$ energy storage cycle originated from the compressed air energy storage (CAES). The CAES system uses excess electricity to compress and store air in off-peak time and generate electricity by heating the compressed air and expanding it during the peak time [13]. To eliminate the need for fossil fuels in the CAES system, Grazzini et al. [14] adopted the thermal energy storage (TES) technology. Thermal energy is stored in the TES and reused to heat compressed air to increase the work output. Jakiel et al. [15] proposed an optimized CAES system named advanced adiabatic compressed air energy storage (AA-CAES) system without using any fossil fuel. Following this, the liquid air energy storage (LAES) system was proposed, which has higher energy storage density [16]. In addition to the compressed air energy storage, the pumped thermal electricity storage (PTES) is another promising technology. Zhang et al. [17] proposed a 10-MW Brayton-cycle-based PTES system with indirect TES and provided a more economical option for the long-term power storage. Furthermore, Wang et al. [18] proposed a TES array with the "temperature complementation" operation mode in the Brayton-cycle-based pumped heat electricity storage. Inspired by the above works, it was also proposed to replace air or water with CO$_2$ as working fluid. Liu et al. [19] found that the critical parameters of CO$_2$ are higher than air so that it is easy to become liquid or supercritical state. Mercangoz et al. [20] proposed an electrothermal energy storage with transcritical CO$_2$ cycles and the pilot system efficiency is up to 51%. Kim et al. [21] proposed isothermal transcritical CO$_2$ cycles based on the TES system and discussed the system performance. Furthermore, Zhang et al. [22] presented the

compressed CO_2 energy storage (CCES) based on transcritical CO_2 Brayton cycle. Then they compared the CCES system, liquid CO_2 system and advanced adiabatic compressed air energy storage (AA-CAES) and found that the CCES has a greater application potential. Liu et al. [11] proposed a two-reservoir supercritical and transcritical compressed CO_2 energy storage system and found that the supercritical compressed CO_2 energy storage configuration is simpler, and the energy density is higher than those of CAES. The work in [11] demonstrates that a supercritical compressed CO_2 energy storage system is quite similar to the S-CO_2 coal-fired Brayton power cycle, in which the compressor, turbine, heater, cooler and recuperator are all present. And the CO_2 fluids are both in a supercritical state in the two cycles.

As mentioned above, most of the efforts are focused on several specific system configurations and different types of system have completely different performance. However, to investigate the sustainability of the coal-fired power plant, the connection and transformation of the different types of the systems based on the coal-fired power system should be unveiled owing to the gradual change in the dominant energy resource type. As a result, this work conducted a feasibility study on how to gradually convert the S-CO_2 coal-fired power cycle into the S-CO_2 energy storage cycle with the gradual elimination of fossil energy for the sustainability of power plants.

The major contributions of this study are as follows.

1) Integration and conversion of supercritical carbon dioxide coal-fired power cycle and high-efficiency energy storage cycle are discussed.

2) A three-step strategy is proposed and various cycles are presented and assessed.

The rest of this paper is organized as follows. A brief cycle description and thermal dynamic model are presented in Section 2. The performance criteria of energy and exergy analyses are introduced in Section 3. In Section 4, the feasibility analysis and a three-step strategy are presented. A brief summary is given in Section 5.

2. Cycle description and thermodynamic model

To accomplish the feasibility analysis of the integration and even conversion of the S-CO_2 coal-fired power cycle and the S-CO_2 energy storage cycle, the basic configurations of the two cycles are introduced briefly in this Section. The introduction of these two cycles provides a good basis for

1   subsequent cycle analysis in Section 4.1.

2   Some assumptions are made to simplify the model:

3   1) The mass flow rate and working time are the same during the charging and discharging.

4   2) The cycle parameters are calculated based on the unit mass flow rate.

5   3) The pressure drop in the recuperator and heater is set at 0.1 MPa.

6   4) The pinch temperature of the recuperator is set at 10 ℃.

7   5) The compressor and the turbine have an isentropic efficiency of 0.89 and 0.9, respectively.

8   6) The kinetic energy and potential energy are negligible in the system.

9   7) Heat and friction losses are negligible in pipes and each component.

10   *2.1 Supercritical carbon dioxide coal-fired power cycle*

11   The basic S-CO$_2$ coal-fired power cycle is a recompression Brayton cycle as shown in Fig. 1 [4].

12   The power cycle consists of a turbine (T), two compressors (C1 and C2), a high temperature

13   recuperator heat exchanger (HTR) and a low temperature recuperator heat exchanger (LTR). Heater

14   represents the furnace cooling wall and flue gas heat exchangers in boiler. The cooler dissipates excess

15   heat to the environment. Moreover, the total flow rate is split into two streams, one goes through C1

16   and the other goes through C2.
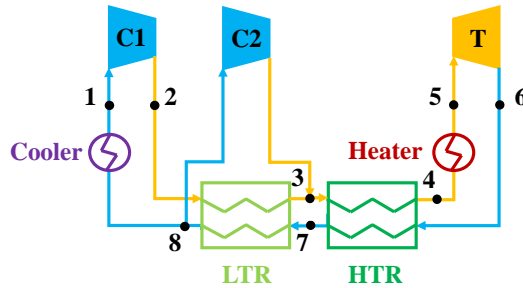
17

18   Fig. 1. The schematic of the S-CO$_2$ recompression Brayton coal-fired power cycle [4].

19   The thermodynamic model of the cycle is as below:

20   The isentropic efficiencies of compressors η_{c1} and η_{c2} are,

$$\eta_{c1} = \frac{h_{2,s} - h_1}{h_2 - h_1}, \ \eta_{c2} = \frac{h_{3,s} - h_8}{h_3 - h_8} \tag{1}$$

22   where $h_{2,s}$ and $h_{3,s}$ are the enthalpies during isentropic compression, respectively, and h_1, h_2, h_3, h_8 are

23   the real enthalpies during compression.

The entropies of the inlet and outlet are the same during the isentropic compression,

$$s_{2,s} = s_1, \ s_{3,s} = s_8 \tag{2}$$

The corresponding outlet enthalpy can be calculated by the equations of state,

$$h_{2,s} = f\left(s_{2,s}, p_2\right), \ h_{3,s} = f\left(s_{3,s}, p_3\right) \tag{3}$$

So, the real enthalpy can be calculated by the definition of compression efficiency. Further, the power consumptions are,

$$W_{c1} = m_{1\text{-}2}\left(h_2 - h_1\right), \ W_{c2} = m_{8\text{-}3}\left(h_3 - h_8\right) \tag{4}$$

The calculation of recuperators is based on the energy conservation equation,

$$m_{7\text{-}8}\left(h_7 - h_8\right) = m_{2\text{-}3}\left(h_3 - h_2\right), \ m_{6\text{-}7}\left(h_6 - h_7\right) = m_{3\text{-}4}\left(h_4 - h_3\right) \tag{5}$$

where $m_{7\text{-}8}$, $m_{6\text{-}7}$ and $m_{2\text{-}3}$, $m_{3\text{-}4}$ are the mass flow rates of S-CO$_2$ on the hot and cold sides, respectively.

As for the split flow, the S-CO$_2$ flow rate extraction ratio χ is defined as the flow rate going through the second compressor divided by the total flow rate. So, the mass flow rates in HTR and LTR are,

$$m_{6\text{-}7} = m_{3\text{-}4} = m_{\text{total}} \tag{6}$$

$$m_{7\text{-}8} = m_{\text{total}} \tag{7}$$

$$\dot{m}_{2\text{-}3} = \left(1 - \chi\right)\dot{m}_{\text{total}} \tag{8}$$

The isentropic efficiency of turbine is,

$$\eta_t = \frac{h_5 - h_6}{h_5 - h_{6,s}} \tag{9}$$

The entropies of the inlet and outlet are the same during the isentropic expansion,

$$s_{6,s} = s_5 \tag{10}$$

The corresponding outlet enthalpy can be calculated by the equation of state,

$$h_{6,s} = f\left(s_{6,s}, P_6\right) \tag{11}$$

Thus, the real enthalpy can be calculated by the definition of expansion efficiency. Further, the expansion work is,

$$W_t = m_{5\text{-}6}\left(h_5 - h_6\right) \tag{12}$$

2.2 Supercritical carbon dioxide energy storage cycle

An S-CO$_2$ energy storage cycle using two storage tanks is a closed energy-storage cycle as schematic in Fig. 2 [11], which has the highest similarity to the S-CO$_2$ coal-fired power cycle available. The energy storage cycle consists of a turbine (T), a compressor (C), a high pressure storage tank (HPT) and a low pressure storage tank (LPT). A heater inputs heat to the system while a cooler dissipates excess heat to environment. A recuperator (RE) is utilized to capture the heat from the turbine exhaust.
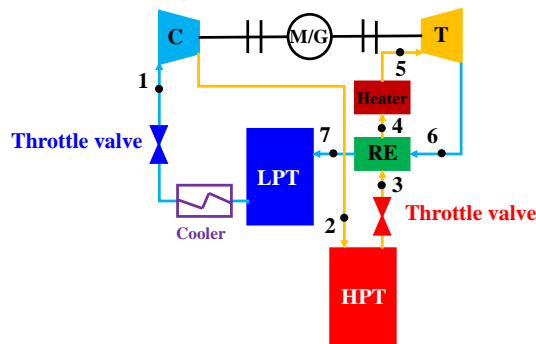
Fig. 2. The schematic of the supercritical compressed CO$_2$ energy storage (SC-CCES) cycle [11].

The thermodynamic model of the cycle is presented as below.

The compressor, turbine and recuperator calculation models are the same as those in the S-CO$_2$ power cycle.

The high pressure storage tank model consists of a storage tank and its corresponding throttle valve. Assume that changes in kinetic energy and potential energy are negligible. The inlet and outlet thermohydraulic parameters of the storage tank can be regarded as the same. Then the throttling process is treated as an isenthalpic expansion process,

$$h_{in,thro} = h_{out,thro} \tag{13}$$

Therefore, the high pressure storage tank calculation model is,

$$h_{in,HPT} = h_{out,thro} \tag{14}$$

However, the low pressure storage tank model consists of not only the storage tank and the corresponding throttle valve, but also the cooler according to the schematic cycle. Thus, both pressure drop in the throttle valve and heat dissipation in the cooler should be considered.

1   **3. Performance criteria**

2   To discuss the performance of the S-CO$_2$ coal-fired power cycle and the S-CO$_2$ energy storage

3   cycle, both the energy and exergy analyses are conducted. For energy analysis, the power cycle

4   efficiency and the round-trip efficiency are representative criteria for the power cycle and the energy

5   storage cycle, respectively [4, 11]. The energy storage density is a typical criterion of compressed

6   energy storage cycle [11]. For exergy analysis, the exergy destruction is a well-known key performance

7   criterion of the main components in the cycle. With all the energy/exergy and cycle/component criteria

8   calculated, the performance can be evaluated.

9   *3.1 Energy analysis*

10   *3.1.1 Power cycle efficiency*

11   The cycle efficiency of the coal-fired power cycle is [6],

12
$$\eta_{power} = \frac{W_t - W_c}{Q_h} \tag{15}$$

13   where W_c is the compression work, W_t is the expansion work, and Q_h is the heat absorption in the

14   boiler.

15   *3.1.2 Round-trip efficiency*

16   The round-trip efficiency of the energy storage cycle is defined as [23, 24],

17
$$\eta_{rt} = \frac{W_t}{\left(W_c + \eta_{pp}Q_h\right)} \tag{16}$$

18   where W_c represents the electricity input, which is the compression work, W_t represents the electricity

19   output, which is the expansion work, $\eta_{pp}Q_h$ is the equivalent amount of electricity, which is converted

20   by the heat absorption Q_h in the heater, η_{pp} is the stand-alone power plant efficiency.

1 *3.1.3 Energy storage density*

2   Energy storage density is also one of the important performance criteria of the cycle, defined as

3 [12, 22],

4
$$\rho_{E} = \frac{W_{t}}{V_{r}} = \frac{W_{t}}{\sum_{k} \dfrac{m_{co_2,k}}{\rho_{co_2,k}}}$$
(17)

5   where V_r is the storage volume, $\dot{m}_{co_2,k}$ is the mass flow rate of S-CO$_2$ in the k$_{th}$ storage tank, and

6 $\rho_{co_2,k}$ is the density in the k$_{th}$ storage tank.

7 *3.2 Exergy analysis*

8   The system exergy balance is [11, 25, 26, 27],

9
$$E_{F,total} = E_{P} + \sum_{i} E_{D,i} + E_{L}$$
(18)

10 where $\dot{E}_{F,total}$, $\dot{E}_{P}$, $\sum_{i} \dot{E}_{D,i}$ and $\dot{E}_{L}$ represent the total rates of fuel exergy, product exergy, exergy

11 destruction and exergy loss in the system, respectively.

12   The exergy balance of the i$_{th}$ component can be expressed as

13
$$E_{D,i} = E_{F,i} - E_{P,i}$$
(19)

14 where $\dot{E}_{D,i}$, $\dot{E}_{F,i}$ and $\dot{E}_{P,i}$ represent the exergy destruction rate, the fuel exergy, and the product exergy

15 rate in the i$_{th}$ component, respectively.

16   To compare the exergy destruction of different components, the exergy destruction ratio is defined

17 as

18
$$y_{D,i}^{*} = \frac{E_{D,i}}{E_{D,total}}$$
(20)

19 *3.3 Validation*

20   The calculation model of the S-CO$_2$ coal-fired power cycle was verified in present authors'

21 previous works [6-10]. The validation of the S-CO$_2$ energy storage cycle is carried out here. The

22 comparison between the present results and the data in [11] is shown in Table 1. The deviations are less

1   than 4.6% in temperature, 3.9% in pressure, 4.4% in enthalpy, 2.9% in entropy, and 2.4% in exergy. A

2   good agreement is found.

3   Table 1. Comparison of cycle parameters of the S-CO$_2$ energy storage cycle.

Stream	$T_{[11]}$ /°C	$T_{present}$ /°C	$P_{[11]}$ /MPa	$P_{present}$ /MPa	$h_{[11]}$ /kJ·kg^{-1}	$h_{present}$ /kJ·kg^{-1}	$s_{[11]}$ /kJ·kg^{-1}·K^{-1}	$s_{present}$ /kJ·kg^{-1}·K^{-1}	$e_{[11]}$ /kJ·kg^{-1}	$e_{present}$ /kJ·kg^{-1}
1	34.7	34.7	7.40	7.40	400.71	400.68	1.66	1.66	228.07	228.07
2	159.5	159.4	40.18	40.18	484.96	484.92	1.69	1.69	302.86	303.24
3	134.3	128.1	20.81	20.00	492.43	484.92	1.80	1.79	276.67	272.61
4	425.9	436.9	20.00	19.90	882.22	895.81	2.54	2.56	437.04	445.33
5	599.9	599.9	20.00	19.80	1097.20	1097.32	2.81	2.82	568.41	567.87
6	490.6	489.7	8.04	8.14	973.57	972.38	2.84	2.83	437.31	437.30
7	114.0	113.1	8.04	8.04	537.87	561.50	2.05	2.11	243.42	249.20

4   **4. Results and discussion**

5   A three-step strategy of integration and conversion of S-CO$_2$ coal-fired power cycle and high

6   efficiency S-CO$_2$ energy storage cycle is discussed and new cycles are presented in this section.

7   *4.1 Comparison of supercritical carbon dioxide coal-fired power cycle and energy storage cycle*

8   To make a comparison between the S-CO$_2$ coal-fired power cycle and the S-CO$_2$ energy storage

9   cycle, some modifications are made in the above-mentioned two cycles in Section 2. The LTR and C2

10 are removed from the S-CO$_2$ coal-fired power cycle in Section 2.1. Therefore, the recompression cycle

11 is simplified into a simple recuperated cycle, which can match the S-CO$_2$ energy storage cycle with a

12 single recuperator in Section 2.2, as shown in Fig. 3a. For the S-CO$_2$ energy storage cycle in Section

13 2.2, the cycle is redrawn to make a clearer comparison as shown in Fig. 3b. It can be observed that the

14 compressor, recuperator, turbine, heater, and cooler are in the same positions of the two cycles, while

15 the high pressure and low pressure storage tanks and their corresponding throttle valves are missing in

16 Fig. 3a. First, the high pressure storage tank and its corresponding throttle valve are added in process

17 2-3 in the energy storage cycle, while there is not any component inserted in process 2-3 in the power

18 cycle. Second, the low pressure storage tank and its corresponding throttle valve are presented on both

sides of the cooler in process 7-1, while only a cooler is arranged in process 7-1 in the power cycle. In general, the S-CO_2 power cycle and the energy storage cycle have much similarity, while the only difference lies in the arrangements of storage tanks and their corresponding throttle valves.

The above analysis prompts the idea and shows the feasibility of the integration and conversion of the S-CO_2 power cycle and the energy storage cycle based on three key points. First, the power cycle can have energy storage function by adding storage tanks. Second, the heating process 4-5 can be achieved by the coal-fired boiler. Third, most key components in the S-CO_2 power cycle can be reused in the S-CO_2 energy storage cycle, such as the compressor, turbine, recuperator, and cooler.
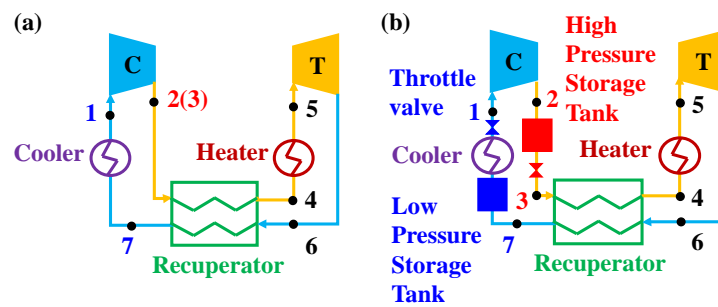
Fig. 3. The schematics of simple recuperated (a) S-CO_2 power cycle and (b) S-CO_2 energy storage cycle.

To make a preliminary comparison, the cycle parameters of the two cycles are calculated based on the same inlet temperature and pressure of compressor and inlet temperature of turbine. Fig. 4 shows the T-S diagrams of the two cycles. The largest divergence appears at the outlet of the compressor. In the S-CO_2 power cycle, the compressor links the recuperator directly without causing huge pressure drop. However, due to the high pressure throttle valve in the S-CO_2 energy storage cycle, the pressure decreases from 40.18 to 20 MPa. Another divergence is caused by the low pressure throttle valve. The pressure drop increases from 0.1 to 0.64 MPa in process 7-1 from the power cycle to the energy storage cycle. These two divergences lead to large changes in the recuperator and turbine. First, the enthalpy exchange in recuperators increases from 266.89 kJ·kg^{-1} in the power cycle to 410.88 kJ·kg^{-1} in the energy storage cycle, which is attributed to the larger temperature difference between inlet and outlet of recuperator in the energy storage cycle. Second, the expansion work of the energy storage cycle is 124.94 kJ·kg^{-1} compared with 220.37 kJ·kg^{-1} in power cycle due to the higher outlet temperature and lower pressure drop of the turbine, which are 489.7 °C / 11.66 MPa in energy storage cycle and 400.0 °C / 32.38 MPa in power cycle, respectively.
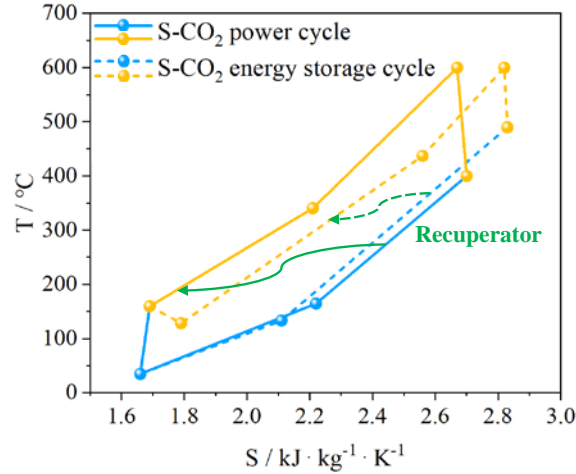
Fig. 4. T-S diagrams of the simple recuperated S-CO$_2$ power cycle and the energy storage cycle.

The energy and exergy are presented for a further comparison. Due to the different definitions of energy performance criteria in power and energy storage cycles, the cycle efficiency of the power cycle is 40.45% calculated by Eq. (15), while the calculated round-trip efficiency of the energy storage cycle is 69.35% by Eq. (16). As for exergy performance criteria, Fig. 5 shows the exergy destruction ratio of the main components. For the S-CO$_2$ power cycle, 37.3% of the irreversibility takes place in the heater, 29.8% in the cooler, 12% in the turbine, 11.2% in the recuperator and 9.6% in the compressor. While for the S-CO$_2$ energy storage cycle, the largest exergy destruction of 29.46% occurs in the high pressure storage tank. The heater, low pressure storage tank and cooler, and recuperator also bring large exergy destruction, which are 21.29%, 20.32% and 14.78%, respectively. It can be observed that the exergy destruction ratio of energy storage tanks accounts for around half.
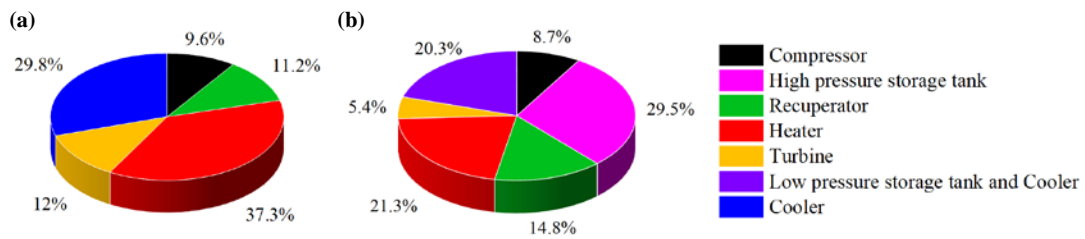
Fig. 5. The exergy destruction ratio of main components of simple recuperated (a) S-CO$_2$ power cycle and (b) S-CO$_2$ energy storage cycle.

Additionally, the throttle valve of the storage tank will cause extra loss of the pressure in the cycle. Therefore, a simple addition of the storage tanks in the power cycle will decrease the intrinsic efficiency of the power cycle due to the pressure drop penalty on efficiency. Thus, it is recommended that the storage tanks can be short-circuited when a power cycle is needed, and reconnected when the energy storage function is needed.

4.2 First step: supercritical carbon dioxide coal-fired power cycle integrated with energy storage cycle

After illustrating the feasibility of integration and conversion of the S-CO$_2$ coal-fired power cycle and the energy storage cycle, it should be recognized that the modifications cannot be made all at once due to the gradual change in the dominant energy resource type in the future. Therefore, a three-step strategy is proposed to establish a new S-CO$_2$ energy storage system based on the coal-fired power system, which is able to utilize coal energy when coal still plays an important role as a dominant energy resource, various heat sources when the dominant energy resource type changes, and electricity for an adiabatic S-CO$_2$ energy storage system without using any extra heat source finally.

The first step integrating the S-CO$_2$ coal-fired power system with the S-CO$_2$ energy storage system is referred to as the integrated coal-fired supercritical compressed CO$_2$ energy storage (C-SC-CCES) system. Fig. 6 shows the brief description of the C-SC-CCES system. In off-peak time, the S-CO$_2$ coal-fired power generation system provides electricity to power the compressor in the S-CO$_2$ energy storage system, in which S-CO$_2$ is stored in the high pressure storage tank. In peak time, the high pressurized S-CO$_2$ is released out of the storage tank, regulated to a certain pressure through the throttle valve, and heated by the coal-fired boiler. Then high temperature and pressure S-CO$_2$ enters the turbine to generate electricity. Especially, the coal-fired boiler can be used to generate electricity both in the power generation system during off-peak time and in the energy storage system during peak time, which significantly simplifies the whole system layout.
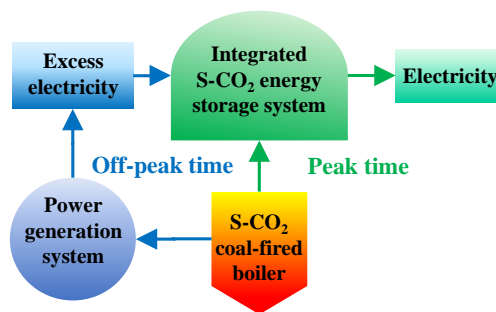
Fig. 6. Schematic of the C-SC-CCES system.

Since the recompression Brayton cycle is usually used in the S-CO$_2$ coal-fired power system, the C-SC-CCES with recompression (C-SC-CCES-RC) cycle is further proposed, as shown in Fig. 7. The difference among the four cases of the C-SC-CCES-RC cycle lies in the arrangement of the storage tanks in process 8-3. The working principle of the C-SC-CCES-RC cycle is presented as follows:

1-2: S-CO$_2$ from LPT is pressurized by compressor using electricity and both the temperature and

pressure of S-CO$_2$ increase.

2-3: S-CO$_2$ is injected into HPT1 and goes through the LTR to absorb thermal energy.

3-4: Two S-CO$_2$ partial flows are combined together and go through HTR to get higher enthalpy.

4-5: S-CO$_2$ is heated in the coal-fired boiler.

5-6: S-CO$_2$ enters the turbine and the turbine drives a generator to produce electricity.

6-7-8: High temperature S-CO$_2$ passes through the HTR and LTR to provide thermal energy.

8-1: S-CO$_2$ total flow is split into two flows and one of them is injected into LPT.

8-3: The other S-CO$_2$ split flow is injected into the second compressor (C2). When there exists no storage tank, S-CO$_2$ split flow goes through C2 straightly. When HPT2 is added in the process, S-CO$_2$ split flow is stored in HPT2 during the off-peak time and removed during the peak time. When LPT2 is added in the process, S-CO$_2$ split flow is stored in LPT2 during the peak time and removed during the off-peak time.
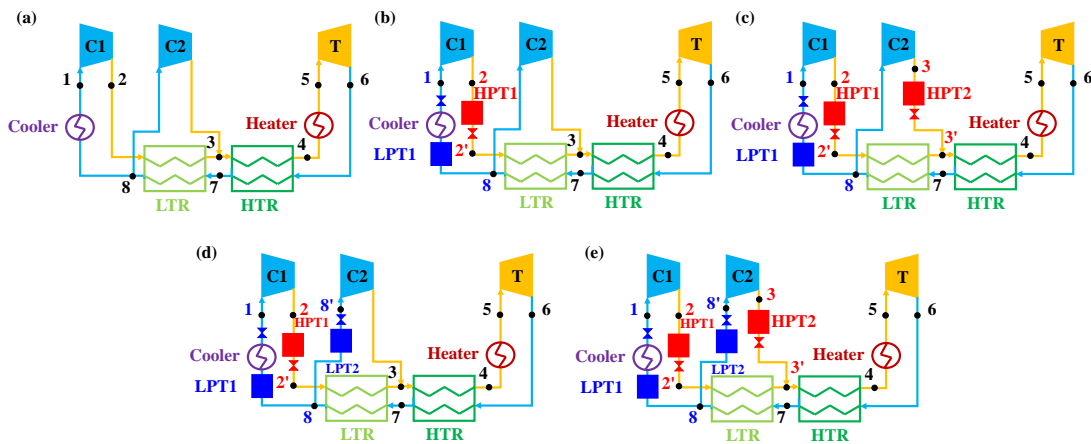
Fig. 7. Schematics of (a) the recompression S-CO$_2$ coal-fired power cycle and the

C-SC-CCES-RC cycle of (b) Case 1, (c) Case 2, (d) Case 3 and (e) Case 4.

The cycle parameters for the four C-SC-CCES-RC cases are calculated and presented in Fig. 8. It can be observed from the T-S diagram that the four cases have similar cycle parameters. The largest difference is caused by the arrangement of high pressure storage tanks as shown in the black box. There occur great pressure drops in the throttle valves behind the HPTs in Case 2 and Case 4, which causes the increase in entropy and decrease in temperature. The influence of low pressure storage tanks is not obvious in these cases due to the low pressure drops of the throttle valves.
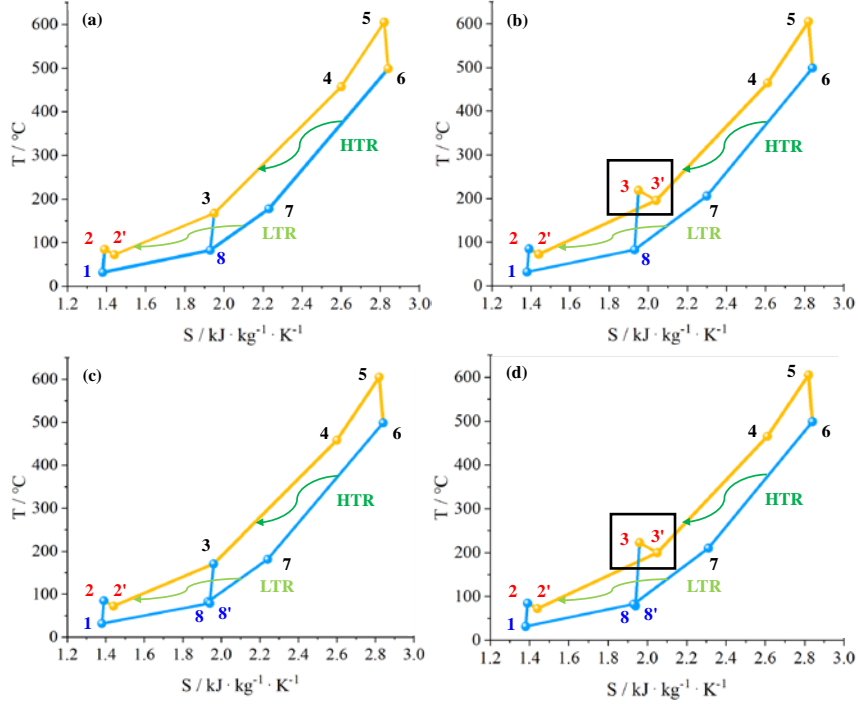
Fig. 8. T-S diagrams of the C-SC-CCES-RC cycle of (a) Case 1, (b) Case 2, (c) Case 3 and (d) Case 4.

The round-trip efficiency is calculated to assess the performance of the four cases. In the C-SC-CCES-RC cycle, Q_h in Eq. (16) is directly provided by the coal-fired boiler. Therefore, the round-trip efficiency of the integrated cycles is modified as below:

$$\eta_{rt,inte} = \frac{W_t}{W_c + Q_h} \tag{21}$$

The round-trip efficiencies of the four cycles are 52.49%, 51.25%, 52.32% and 51.08%, respectively. Case 1 has the largest efficiency, followed by Case 3, Case 2 and Case 4 in sequence. It is because the addition of HPT and LPT causes pressure drops in the cycle, which reduces the efficiency. Especially, HPT has larger pressure drop, which causes larger penalty on efficiency. Therefore, Case 4 with both HPT and LPT has the lowest efficiency, while Case 3 with only LPT has the second highest efficiency.

The energy storage densities of the four cycles are 7.34, 5.88, 4.82 and 4.24 kWh·m^{-3}, respectively. It can be observed that Case 1 has the largest energy storage density owing to only two storage tanks. The energy storage density drops due to the addition of HPT and LPT. Meanwhile, HPT has higher energy storage density than LPT. Therefore, Case 2 has the second highest energy storage density,

1   followed by Case 3 and Case 4 in sequence.

2   As for exergy performance criteria, Fig. 9 shows the exergy destruction ratios of the main

3   components of the four cases. Most of the irreversibility takes place in the heater, which accounts for

4   around 20-30% in each case. Moreover, due to the addition of HPT and LPT, the exergy destruction

5   ratio of storage tanks increases. It can be observed that the storage tanks are becoming the main exergy

6   destruction components, and the proportion increases from 35.32% in Case 1 to 55.48% in Case 4.
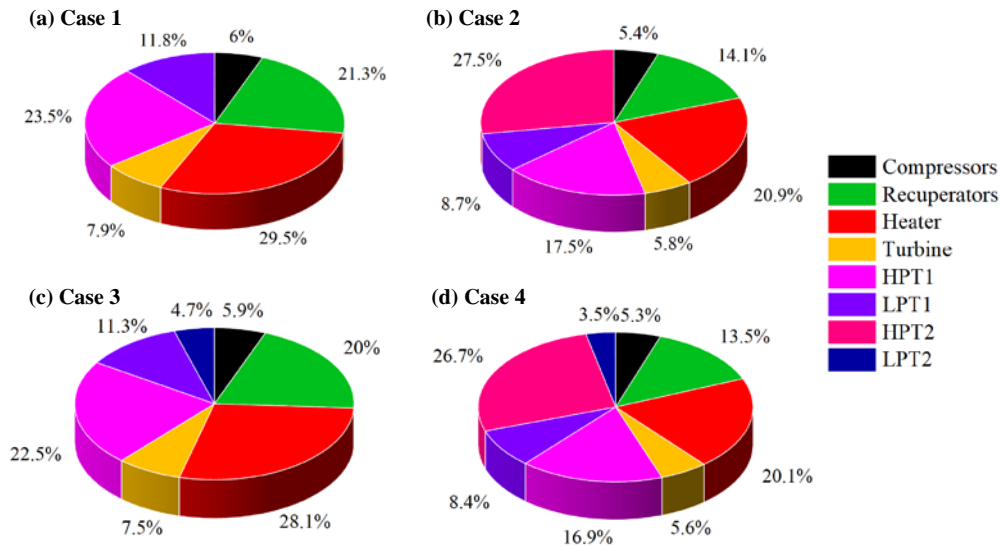
7

8   Fig. 9. Exergy destruction ratios of main components of the C-SC-CCES-RC cycle of (a) Case 1,

9   (b) Case 2, (c) Case 3 and (d) Case 4.

10   In summary, Case 1 has the highest round-trip efficiency, energy storage density and exergy

11   destruction performance. Therefore, it can be regarded as the best configuration of the C-SC-CCES-RC

12   cycle. Since the storage tank in the extraction process not only increases system complexity, but also

13   causes pressure drop penalty on the cycle efficiency, careful attention should be paid to adding the

14   storage tank in different positions of the cycle.

15   Moreover, instead of adding turbines, the construction of multi-compression is also effective for

16   cycle efficiency improvement [28]. Therefore, inspired by the multi-compression S-CO$_2$ coal-fired

17   power cycles, a possibility to increase efficiency by adding the compression stage in the C-SC-CCES

18   cycle is considered.

19   Based on Case 1, the tri-compression cycle is considered, which is abbreviated as the

20   C-SC-CCES-TC. Fig. 10 shows the schematic of C-SC-CCES-TC. Similar to the working principle of

21   the C-SC-CCES-RC, S-CO$_2$ is compressed and stored in the high pressure storage tank, then heated

and expanded in turbine to generate electricity. Particularly, MTR and C3 are added in the cycle. Fig. 11 shows the T-S diagram of the cycle. The inlet temperatures of HPT1 and LPT1 are lower than 100 °C. It is because that the S-CO$_2$ storage tanks are constructed at the bottom of the cycle, where the cycle parameters are low. This configuration results in lower tank temperatures and increases the thermal safety of the tank. Besides, the inlet temperature of the turbine is 605 °C owing to the heat absorption in the coal-fired boiler and the heat recovery in the recuperators. The round-trip efficiency is 56.37% and the energy storage density is 8.59 kWh·m^{-3}, which are both higher than those of the recompression cycle. In the tri-compression cycle, the total mass flow, scaled as m_{total} kg/s, goes through the turbine and the heater. However, owing to the three compressors existed, the three partial flows which go through each compressor are $\left(1-\chi_2\right)\left(1-\chi_3\right)m_{total}$ in C1, $\chi_2\left(1-\chi_3\right)m_{total}$ in C2 and

$\chi_3 m_{total}$ in C3 as shown in Fig. 10, where $\chi_2=1-\dfrac{h_9-h_{10}}{h_3-h_{2'}}$, $\chi_3=1-\dfrac{h_8-h_9}{h_4-h_3}$, respectively. Therefore,

the expansion work is $W_t=m_{total}\left(h_6-h_7\right)$, while the compression works are

$W_{c1}=\left(1-\chi_2\right)\left(1-\chi_3\right)m_{total}\left(h_2-h_1\right)$ in C1, $W_{c2}=\chi_2\left(1-\chi_3\right)m_{total}\left(h_3-h_{10}\right)$ in C2, and $W_{c3}=\chi_3 m_{total}\left(h_4-h_9\right)$

in C3. The increase in the number of the partial flow leads a decrease of the mass flow rate in each compressor, which brings a decrease of the compression work. Meanwhile, the expansion work is based on the total mass flow, which is not affected by partial flow. Therefore, comparing to the recompression cycle which has only two partial flows, the tri-compression cycle has a higher round-trip efficiency. Besides, the energy storage density increases owing to the decrease in mass flow rate in process 10-2', i.e., C1. Furthermore, Fig. 12 shows the exergy destruction ratio of main components of the C-SC-CCES-TC cycle. It is obvious that the ratio is similar to that in Fig. 9a. Therefore, the C-SC-CCES-TC cycle can be regarded as an improved configuration of the integrated cycle, which has advantages in achieving efficient engineering applications.
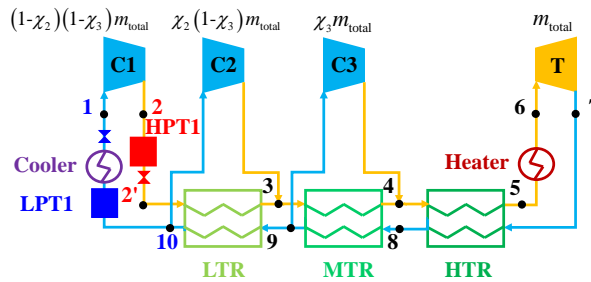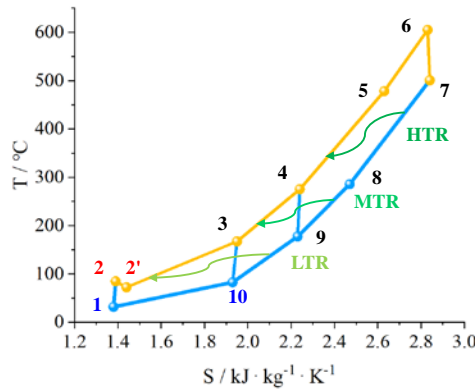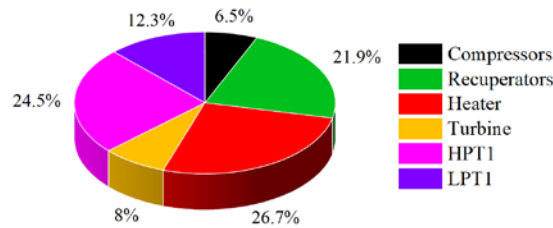
Fig. 11. T-S diagram of the C-SC-CCES-TC cycle.

Fig. 12. Exergy destruction ratio of main components of the C-SC-CCES-TC cycle.

For clearer understanding of the C-SC-CCES cycles, the exergy flow diagrams showing charging, storage and discharging of the recompression (RC) and the tri-compression (TC) cycle are depicted in Fig. 13. The TC cycle has one more compressor and one more recuperator than the RC cycle. The product specific exergy of the compressors in the TC cycle is higher than that in the RC cycle, while the fuel specific exergy of the turbine in the TC cycle is lower than that in the RC cycle. When the specific exergy is multiplied by the corresponding mass flow rate in each stream, the round-trip efficiency of the TC cycle is higher than that of the RC cycle. χ in the RC cycle is 0.3881, χ_2 and χ_3 in the TC cycle are 0.3885 and 0.1600, respectively. Besides, the stored and released specific exergies of the storage tank are the same in the two cycles. Owing to the much lower mass flow rate of the energy storage process in the TC cycle, its energy storage density is much higher than that of the RC cycle based on Eq. (17).
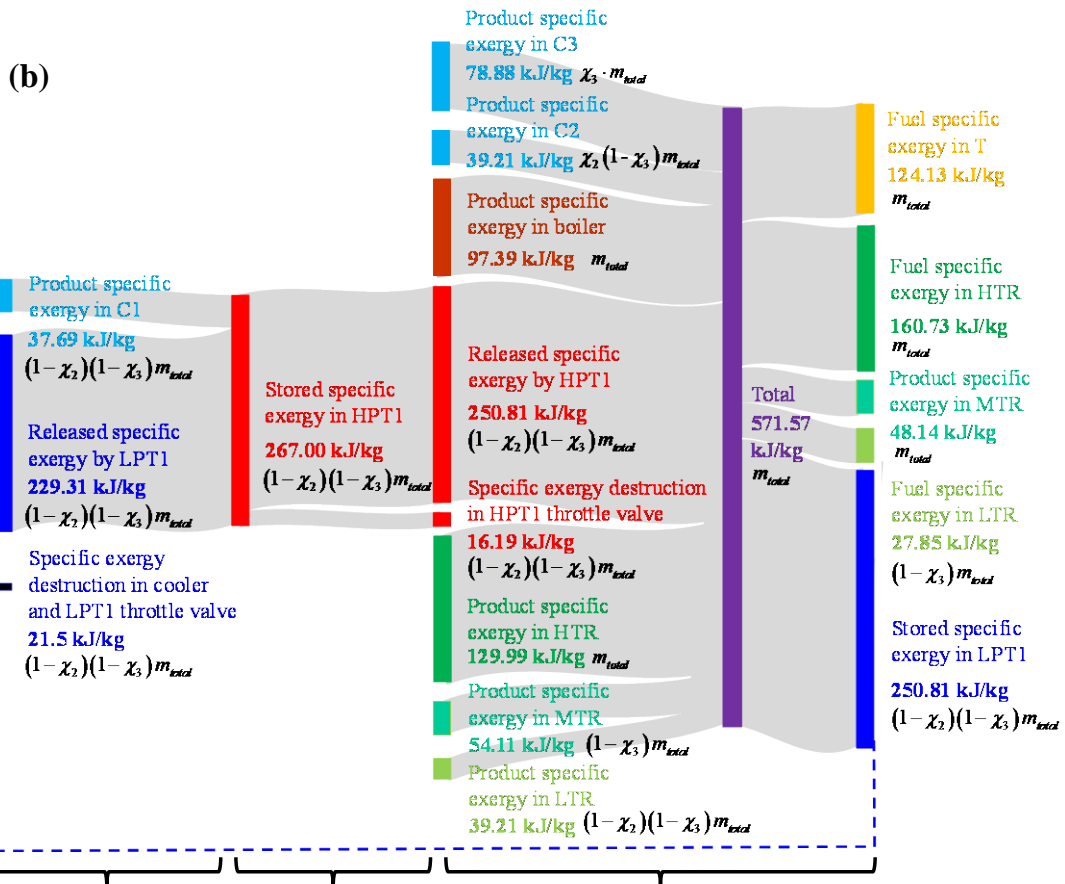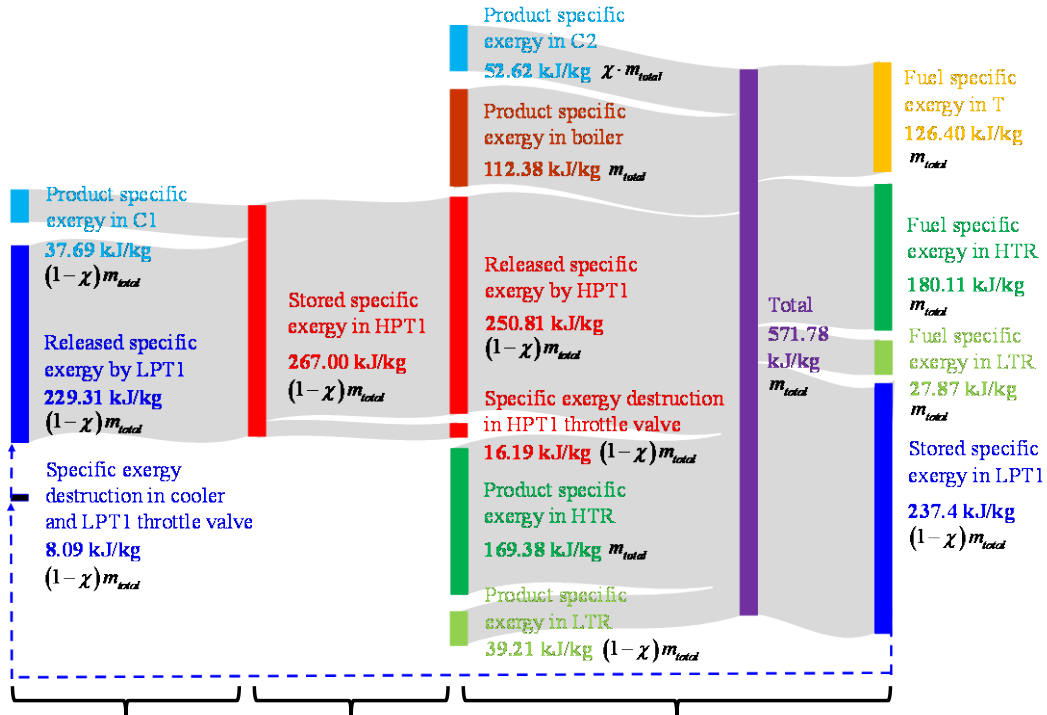
Fig. 13. Exergy flow diagrams in (a) the recompression and (b) the tri-compression cycles during

charging and discharging.

Additionally, the environmental analysis of the recompression and tri-compression integrated coal-fired supercritical compressed CO_2 energy storage systems is conducted. The CO_2, SO_2 emission which is produced by the boiler is investigated. The anthracite coal is used, and the properties are shown in Table 2 [4]. According to the coal complete combustion calculation [29], the environmental performance of the two systems is unveiled in Table 3. The recompression system produces 9.51×10^{-3} kg of CO_2, 3.47×10^{-5} kg of SO_2 per unit mass flow rate of working fluid, while the tri-compression system reduces the CO_2 and SO_2 emissions to 8.18×10^{-3} and 2.98×10^{-5} kg per unit mass flow rate, respectively. This is because that the heat load of the tri-compression system is lower, which leads to less coal and the emissions.

Table 2. Properties of the anthracite coal [4].

C_{ar}	H_{ar}	O_{ar}	N_{ar}	S_{ar}	A_{ar}	M_{ar}	V_{daf}	$Q_{net,ar}$
61.70	3.67	8.56	1.12	0.60	8.80	15.55	34.73	23442

C (carbon), H (hydrogen), O (oxygen), N (nitrogen), S (sulfur), A (ash), M (moisture),V (Volatile), ar, daf means as received, dry and ash free, $Q_{net,ar}$ means low heat value of coal (kJ·kg^{-1}).

Table 3. Environmental analysis of the recompression and tri-compression integrated coal-fired supercritical compressed CO_2 energy storage systems.

System	CO_2 (m^3·kg^{-1})	SO_2 (m^3·kg^{-1})	Reduced CO_2 (m^3·kg^{-1})	Reduced SO_2 (m^3·kg^{-1})
Recompression	9.51×10^{-3}	3.47×10^{-5}	0	0
Tri-compression	8.18×10^{-3}	2.98×10^{-5}	1.33×10^{-3}	4.87×10^{-6}

Note that there exist different coal-fired power systems, so the power systems can also be changed into different C-SC-CCES systems. For example, the schematic of the tri-compression integrated coal-fired supercritical compressed CO_2 energy storage system is depicted in Fig. 14, which shows how coal energy provides heat for the system. The effect of the coal-fired boiler is to improve the inlet parameters of the turbine and generate a temperature difference in the recuperators to achieve the heat recovery process. Furthermore, the existence of the S-CO_2 storage block brings the energy storage function of the integrated system.
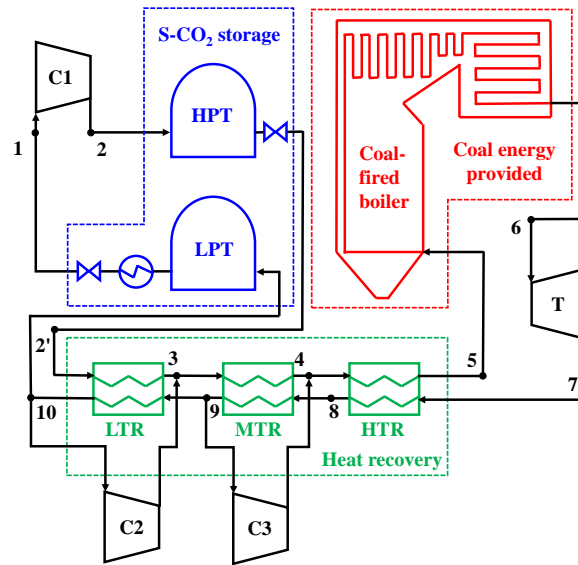
Fig. 14. Schematic of the tri-compression integrated coal-fired supercritical compressed CO_2 energy storage system.

4.3 Second step: integrated supercritical carbon dioxide energy storage cycle with various heat sources

Along with the challenge in coal energy utilization in the future, three conditions are assessed. First, peak-shaving is one of the main challenges facing coal-fired power system. Second, the coal-fired boiler may be changed into biomass boiler or refuse incineration boiler. Third, the boiler may be modified into other heating equipment such as solar energy heater, geothermal energy heater and so on. Therefore, the integrated S-CO_2 energy storage cycle should adapt to different heat loads due to the various heat sources available in future. The heat load in the integrated cycle may come from complex sources, e.g. a single heat source or hybrid heat sources, which can be either higher or lower than that of the coal-fired boiler.

Detailed assessment of the heat sources in the above three conditions is given here. First, when the coal-fired power system is in peak-shaving condition, the heat load of the boiler will decrease. The heat load of the boiler in the TC cycle is 157.24 kJ·kg^{-1}, as calculated in Section 4.2. Therefore, the case of lower heat load should be investigated. Second, the biomass boiler and the refuse incineration boiler have lower heat load than the coal-fired boiler as is well known, which also need to be considered. Third, when other heating equipment is used alone in the system, the heat load hardly exceeds that of the coal-fired boiler. However, if the integrated system uses hybrid heat sources rather than a single heat source, e.g. the coal-fired boiler combined with the biomass boiler or the refuse incineration boiler,

the solar energy heater combined with the geothermal energy heater, etc., the heat load in the system is likely to exceed that of the coal-fired boiler. Therefore, the case of higher heat load also should be investigated. As a result, the scale of the heat load is set from around 100 to 200 kJ·kg^{-1} for further analysis.

Based on the C-SC-CCES system, the supercritical compressed CO_2 energy storage (X-SC-CCES) system integrated with various heat sources is proposed as shown in Fig. 15a. "X" means various methods for heating. In the X-SC-CCES system, the coal-fired boiler is replaced with various heating equipment, which is only used in peak time. The excess electricity is produced by various power generation systems rather than the coal-fired power plant only in off-peak time. The tri-compression integrated cycle is called the X-SC-CCES-TC cycle as schematic in Fig. 15b.
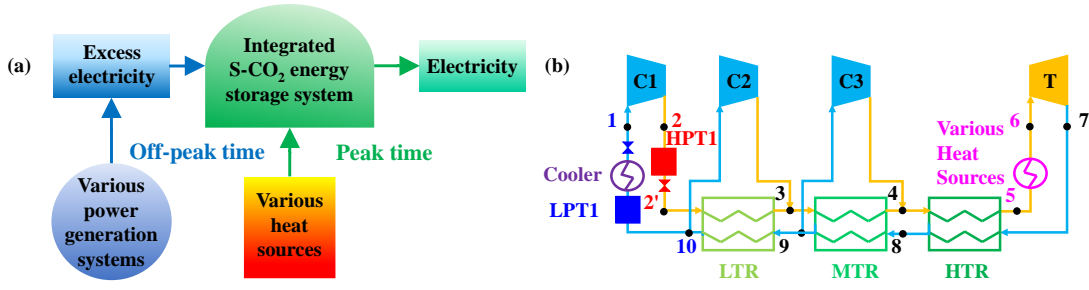
Fig. 15. Schematics of (a) the X-SC-CCES system and (b) the X-SC-CCES-TC cycle.

To investigate the effects of heat load on the X-SC-CCES-TC, the round-trip efficiency and energy storage density are calculated as shown in Fig. 16. First, the round-trip efficiency increases from 50.75% to 58.25% with the increase in heat load from 103.01 to 193.01 kJ·kg^{-1}. It is because higher heat load means higher output work of the turbine. When the power consumption of the compressor is much less than the increase in power output of the turbine, a higher round-trip efficiency is obtained. Second, the energy storage density increases from 6.52 to 9.55 kWh·m^{-3}. According to Eq. (17), the energy storage density is determined by the power output of the turbine and the volume of the two energy storage tanks. A high heat load means a high energy storage pressure, which will increase the density of the S-CO_2 and reduce the required volume of the high-pressure storage tank. Meanwhile, the power output of the turbine increases. Therefore, the energy storage density will increase due to the rise of heat load in the heater.
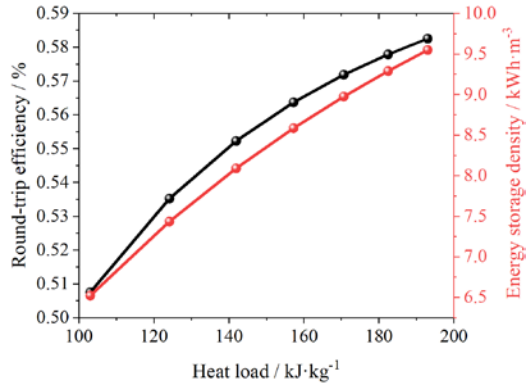
Fig. 16. Effect of heat load on round-trip efficiency and energy storage density.
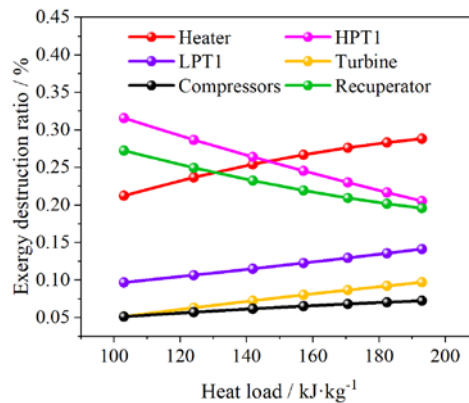
The effect of the heat load on the exergy destruction ratio of main components is shown in Fig. 17. The results indicate that the exergy destruction is mainly contributed from heater, HPT1 and recuperators. Moreover, the heater exergy destruction ratio increases with the increase in the heat load, whereas the change in exergy destruction ratio in HPT1 and recuperators is opposite to that of the heater in the cycle. The exergy destruction of recuperators is mainly contributed by the temperature difference between inlet and outlet of the hot and cold working fluids. The heater exergy destruction is not only contributed by the temperature difference between inlet and outlet of the fluid, but also by the amount of heat load input into the heater. Therefore, there occurs more irreversibility in the heater by the rise of heat load, whereas that of the recuperators will exhibit an opposite trend due to a lower temperature difference between the hot and cold S-CO$_2$. The exergy destruction ratio in HPT1 is caused by the temperature difference between the inlet and outlet of the storage tank, which decreases with the rise of the heat load. However, the exergy destruction ratio in LPT1 increases due to a higher temperature difference. In addition, the exergy destruction ratios of the compressor and turbine increase due to the higher pressure differences in these two components.


Fig. 17. Effect of heat load on exergy destruction ratio on main components.

1   In summary, a trade-off must be struck among the increase in round-trip efficiency, energy storage

2   density and exergy destruction ratio of the heater. This work provides a guidance for examining a

3   suitable heat source for the X-SC-CCES system.

4   *4.4 Third step: adiabatic supercritical carbon dioxide energy storage cycle*

5   When all the heat sources are removed due to their large exergy destruction ratios, the integrated

6   system will be converted into an adiabatic $S-CO_2$ energy storage system. Inspired by the name of

7   AA-CAES [30], this converted system is called the A-SC-CCES system as shown in Fig. 18. "A"

8   means adiabatic. This adiabatic energy storage system eliminates the requirement for extra heat sources.

9   The excess electricity is stored in the energy storage system in off-peak time. In peak time, the

10   A-SC-CCES system can produce electricity without using any extra heat source.
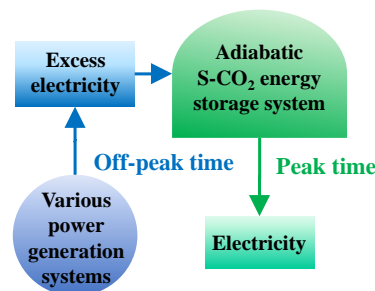
11

12   Fig. 18. Schematic of the A-SC-CCES system.

13   The removal of heat sources causes large changes in the A-SC-CCES cycle. The arrangement of

14   recuperator has to be modified, since no thermal energy is absorbed before the turbine inlet as well as

15   no temperature difference between turbine outlet and cold side outlet of the recuperator. Therefore, the

16   previous recuperator is moved to process 2-5 as shown in Fig. 19a, where the positive temperature

17   difference appears between the inlet of the HPT and outlet of the throttle valve. Fig. 19a shows the

18   schematic of the simple recuperated cycle (A-SC-CCES-SR). $S-CO_2$ is compressed in compressor,

19   provides thermal energy in recuperator and then is stored in HPT. Finally, it is heated by the recuperator

20   and injected into turbine for electricity generation. The recompression cycle (A-SC-CCES-RC) is

21   shown in Fig. 19b. Furthermore, inspired by [31], the throttle valve is replaced with pressure stabilized

22   turbine in split expansion cycle (A-SC-CCES-SE) as schematic in Fig. 19c. The $S-CO_2$ is injected into

23   pressure stabilized turbine (T2) to generate electricity rather than go through the throttle valve.
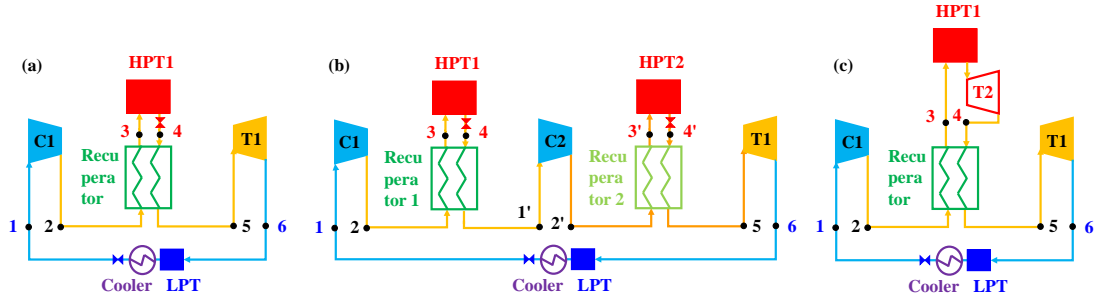
Fig. 19. Schematics of (a) the A-SC-CCES-SR cycle, (b) the A-SC-CCES-RC cycle and (c) the
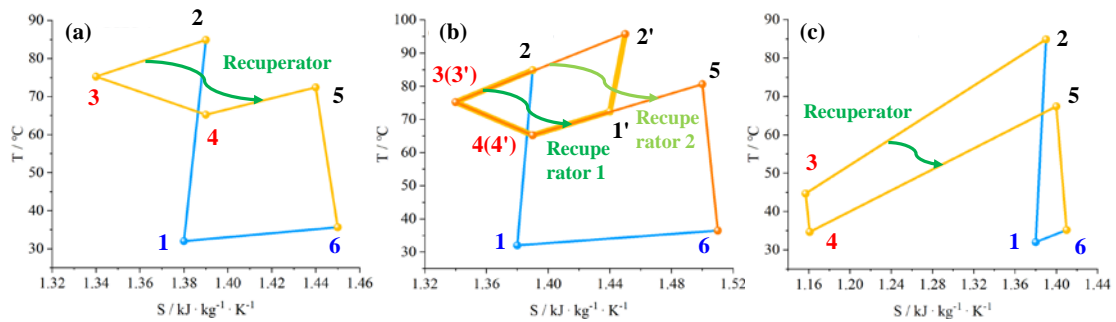
A-SC-CCES-SE cycle.

Fig. 20 shows the T-S diagrams of the A-SC-CCES cycles. It is observed that the maximum

temperature of the cycles is around 85 ℃, which is much lower than that of around 600 ℃ in the

C-SC-CCES cycles as shown in Fig. 8 and Fig. 11. It is because in the A-SC-CCES cycles, no extra

heat load is input in the cycle, and the maximum temperature of the cycles is based on the outlet

temperature of compressor. Since the outlet temperature of the compressor is limited to a low degree,

the maximum temperature of the A-SC-CCES cycles is also low. In addition, the A-SC-CCES-RC

cycle has higher maximum temperature than that of the A-SC-CCES-SR cycle, which is attributed to

that the second compressor in the cycle can increase the compressor outlet temperature to some extent.

Therefore, the turbine inlet temperature increases from 72.4 to 80.6 ℃ as shown in Figs. 20a and 20b.

However, the round-trip efficiency of the A-SC-CCES-RC cycle is 32.43%, which is much lower

than 43.84% in the A-SC-CCES-SR cycle, since the compression work in the A-SC-CCES-RC cycle is

about twice as large as that in the A-SC-CCES-SR cycle due to the existence of two compressors.

However, the expansion work only increases from 18.26 to 20.51 kJ·kg^{-1}, which is much less than the

expected increment, i.e. a factor of 2. Therefore, the round-trip efficiency is reduced.

To improve the round-trip efficiency of the A-SC-CCES cycles, the A-SC-CCES-SE is proposed

as shown in Fig. 19c. By replacing the throttle valve with pressure stabilized turbine, the expansion

work is generated by the two turbines T1 and T2, which is increased to 30.12 kJ·kg^{-1}, while the

compression work is the same as that in the A-SC-CCES-SR cycle. Therefore, the round-trip efficiency

improves to 72.34%.

Besides, the energy storage densities of the three cycles are 1.51, 1.14, and 1.58 kWh·m^{-3},

respectively. The A-SC-CCES-SE cycle has the highest energy storage density due to the largest

expansion work among the three cycles. The A-SC-CCES-SR cycle has larger energy storage density

than the A-SC-CCES-RC cycle due to the only one HPT in the cycle.

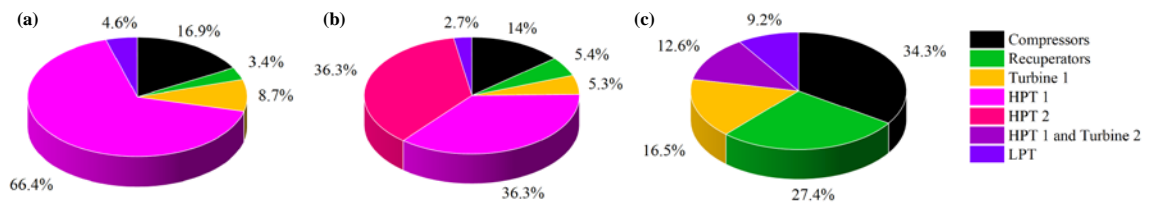Fig. 20. T-S diagrams of (a) the A-SC-CCES-SR cycle, (b) the A-SC-CCES-RC cycle and (c) the

A-SC-CCES-SE cycle.

The exergy destruction ratios of the key components in the three cycles are shown in Fig. 21. Note

that HPT1 and T2 are regarded as a whole in the A-SC-CCES-SE cycle, assuming without change in

parameters in HPT1. It is clear that most of the irreversibility takes place in HPTs in the

A-SC-CCES-SR and the A-SC-CCES-RC cycles, which are 66.4% and 72.6%, respectively. However,

in the A-SC-CCES-SE cycle, the exergy destruction ratio of HPT1 and T2 is 12.6%. Larger exergy

destruction appears in the compressor, recuperator and turbine.

Fig. 21. Exergy destruction ratios of key components of (a) the A-SC-CCES-SR cycle, (b) the

A-SC-CCES-RC cycle and (c) the A-SC-CCES-SE cycle.

For clearer understanding of the addition of the pressure stabilized turbine, the exergy flow

diagrams for charging, storage and discharging of the simple recuperated (SR) cycle and the split

expansion (SE) cycle are depicted in Fig. 22. Owing to T2 in the SE cycle, the released specific exergy

from HPT1 and specific exergy destruction in HPT1 throttle valve are replaced by the released specific

exergy from T2 and fuel specific exergy in T2 as shown in Fig. 22, respectively. The SE cycle has

larger fuel exergy in the turbines but the same product exergy in the compressor as the SR cycle, which

leads to higher round-trip efficiency of the SE cycle. In addition, the higher fuel exergy in the turbines

results in a higher energy storage density in the SE cycle.

(a)

Product specific exergy in C1
37.69 kJ/kg

Released specific exergy by LPT1
229.31 kJ/kg

Specific exergy destruction in cooler and LPT1 throttle valve
1.09 kJ/kg

Total 1
267.00 kJ/kg

Stored specific exergy in HPT1
264.46 kJ/kg

Product specific exergy in recuperator
2.54 kJ/kg

Released specific exergy by HPT1
248.93 kJ/kg

Specific exergy destruction in HPT1 throttle valve
15.53 kJ/kg

Fuel specific exergy in recuperator
1.74 kJ/kg

Specific exergy destruction in recuperator
0.8 kJ/kg

Total 2
250.67 kJ/kg

Fuel specific exergy in T1
20.27 kJ/kg

Stored specific exergy in LPT1
230.40 kJ/kg

Charging   **Storage**   **Discharging**

(b)

Product specific exergy in C1
37.69 kJ/kg

Released specific exergy by LPT1
229.31 kJ/kg

Specific exergy destruction in cooler and LPT1 throttle valve
1.06 kJ/kg

Total 1
267.00 kJ/kg

Stored specific exergy in HPT1
260.00 kJ/kg

Product specific exergy in recuperator
7.00 kJ/kg

Released specific exergy by T2
245.50 kJ/kg

Fuel specific exergy in T2
14.50 kJ/kg

Fuel specific exergy in recuperator
3.84 kJ/kg

Specific exergy destruction in recuperator
3.16 kJ/kg

Total 2
249.34 kJ/kg

Fuel specific exergy in T1
18.97 kJ/kg

Stored specific exergy in LPT1
230.37 kJ/kg

Charging   **Storage**   **Discharging**

Fig. 22. Exergy flow diagrams in (a) the simple recuperated and (b) the split expansion cycle during charging and discharging.

In summary, the A-SC-CCES-SE cycle has the highest round-trip efficiency and energy storage density as well as the lowest exergy destruction ratio in storage tanks, which is recommended for the A-SC-CCES system.

5. Conclusions

In this work, the integration and even conversion of the $S\text{-}CO_2$ coal-fired power cycle and the $S\text{-}CO_2$ energy storage cycle was proposed by a three-step strategy for the sustainability of the power plant. Performance criteria were investigated to assess various newly proposed $S\text{-}CO_2$ energy storage cycles.

1) The first step: when coal still plays an important role as a main energy resource, the C-SC-CCES-TC cycle has the highest round-trip efficiency of 56.37%, and the highest energy storage density of 8.59 kWh·m^{-3}, which can be regarded as the best configuration of the integrated cycle.

2) The second step: with the challenge in utilization of coal energy, a trade-off must be struck among the increase in round-trip efficiency, energy storage density and exergy destruction ratio of heater to find a suitable heat source for the X-SC-CCES system.

3) The third step: when all the heat sources are removed, the A-SC-CCES-SE cycle is recommended by replacing the throttle valve with a pressure stabilized turbine, and a high round-trip efficiency of 72.34% is achieved.

Note that the cycle calculation results in this work are all based on the assumption of unit mass flow rate, which is independent of the system capacity. Therefore, more specific capacity-dependent configurations for the three-step strategy need to be further investigated based on this work. In addition, for practical application, thermo-economic [17] and more in-depth environmental analyses of a specific system are also essential that should be addressed in the future.

References

[1] Li Z, Liu X, Shao Y, Zhong W. Research and development of supercritical carbon dioxide coal-fired power systems. J Therm Sci 2020; 29:546-75.

[2] Mecheri M, Le Moullec Y. Supercritical CO_2 Brayton cycles for coal-fired power plants. Energy 2016; 103:758-71.

[3] Le Moullec Y. Conceptual study of a high efficiency coal-fired power plant with CO_2 capture using a supercritical CO_2 Brayton cycle. Energy 2013; 49:32-46.

[4] Xu J, Sun E, Li M, Liu H, Zhu B. Key issues and solution strategies for supercritical carbon dioxide coal fired power plant. Energy 2018; 157:227-46.

[5] Sun E, Xu J, Hu H, Li M, Miao Z, Yang Y, Liu J.Overlap energy utilization reaches maximum efficiency for S-CO_2 coal fired power plant: A new principle. Energy Convers Manag 2019; 195:99-113.

[6] Fan YH, Tang GH, Yang DL, Li XL, Wang SQ. Integration of S-CO_2 Brayton cycle and coal-fired boiler: Thermal-hydraulic analysis and design. Energy Convers Manag 2020; 225:113452.

[7] Fan YH, Yang DL, Tang GH, Sheng Q, Li XL. Design of S-CO_2 coal-fired power system based on the multiscale analysis platform. Energy 2022; 240:122482.

[8] Li XL, Tang GH, Fan YH, Yang DL. A performance recovery coefficient for thermal-hydraulic evaluation of recuperator in supercritical carbon dioxide Brayton cycle. Energy Convers Manag 2022; 256:115393.

[9] Yang DL, Tang GH, Fan YH, Li XL, Wang SQ. Arrangement and three-dimensional analysis of cooling wall in 1000 MW S–CO_2 coal-fired boiler. Energy 2020; 197:117168.

[10] Yang DL, Tang GH, Li XL, Fan YH. Capacity-dependent configurations of S–CO_2 coal-fired boiler by overall analysis with a unified model. Energy 2022; 245: 123246.

[11] Liu H, He Q, Borgia A, Pan Lehua, Oldenburg C. Thermodynamic analysis of a compressed carbon dioxide energy storage system using two saline aquifers at different depths as storage reservoirs. Energy Convers Manag 2016: 127:149-159.

[12] Wang M, Zhao P, Wu Y, Dai Y. Performance analysis of a novel energy storage system based on liquid carbon dioxide. Appl Therm Eng 2015; 91:812–23.

[13] Lund H, Salgi G. The role of compressed air energy storage (CAES) in future sustainable energy systems. Energy Convers Manage 2009; 50(5):1172–9.

[14] Grazzini G, Milazzo A. Thermodynamic analysis of CAES/TES systems for renewable energy plants, Renew. Energy 2008; 33:1998-2006.

[15] Jakiel C, Zunft S, Nowi A. Adiabatic compressed air energy storage plants for efficient peak load power supply from wind energy: the European project AACAES. Int. J. Energy Technol. Policy 2007; 5:296-306.

[16] Morgan R, Nelmes S, Gibson E, Brett G. Liquid air energy storage e analysis and first results from a pilot scale demonstration plant. Appl. Energy 2015; 137:845-853.

[17] Zhang H, Wang L, Lin X, Chen H. Technical and economic analysis of Brayton-cycle-based pumped thermal electricity storage systems with direct and indirect thermal energy storage. Energy 2022; 239:121966.

[18] Wang L, Lin X, Zhang H, Peng L, Chen H. Brayton-cycle-based pumped heat electricity storage with innovative operation mode of thermal energy storage array. Appl Energy 2021; 291:116821.

[19] Liu H, Chen Y, Xu L, Wang C, Tan C. A solar energy storage and power generation system based on supercritical carbon dioxide. Renew. Energy 2014; 64:43-51.

[20] Mercangoz M, Hemrle J, Kaufmann L, Z'Graggen A, Ohler C. Electrothermal energy storage with transcritical CO_2 cycles. Energy 2012; 45:407-415.

[21] Kim Y, Shin D, Lee S, Favrat D. Isothermal transcritical CO_2 cycles with TES (thermal energy storage) for electricity storage. Energy 2013; 49:484-501.

[22] Zhang Y, Yang K, Hong H, Zhong X, Xu J. Thermodynamic analysis of a novel energy storage system with carbon dioxide as working fluid. Renew. Energy 2016; 99:682-697.

[23] Succar, Samir, Williams Robert H. Compressed air energy storage: theory, resources, and applications for wind power. Report no. 8. Princeton Environmental Institute 2008.

[24] Kim YM, Lee JH, Kim SJ, Favrat D. Potential and evolution of compressed air energy storage: energy and exergy analyses. Entropy 2012; 14(8):1501–21.

[25] Liu H, He Q, Saeed SB. Thermodynamic analysis of a compressed air energy storage system through advanced exergetic analysis. J Renew Sustain Energy 2016; 8(3):034101.

[26] Wang L, Yang Y, Morosuk T, Tsatsaronis G. Advanced thermodynamic analysis and evaluation of a supercritical power plant. Energies 2012; 5(6):1850–63.

[27] Narendran G, Bhat M, Akshay L, Perumal D. Experimental analysis on exergy studies of flow through a minichannel using Tio_2/Water nanofluids. Therm Sci Eng Prog 2018; 8:93-104.

[28] Sun E, Xu J, Li M, Li H, Liu C, Xie J. Synergetics: The cooperative phenomenon in multi-compressions S-CO_2 power cycles. Energy Convers Manag: X 2020; 7:100042.

[29] Che D. Boilers-Theory Design and Operation. Xi'an: Xi'an Jiaotong University Press; 2008.

[30] Zunft S, Jakiel C, Koller M, Bullough C. Adiabatic compressed air energy storage for the grid integration of wind power. Sixth International Workshop on Large-Scale Integration of Wind Power and Transmission Networks for Offshore Windfarms 2006.

[31] Zhang Y. Study on system integration and simulation of wind power and advanced adiabatic compressed air energy storage technology. Institute of Engineering Thermophysics Chinese Academy of Sciences 2014.

1